# THREE-DIMENSIONAL ASPECTS OF SUB-CRITICAL FLAW GROWTH

**C. W. Smith and G. Nicoletto**

*Virginia Polytechnic Institute & State University, Blacksburg, VA 24061, USA*

ABSTRACT

By combining the principles of linear elastic fracture mechanics with the methods of frozen stress photoelasticity and moire analysis, a general experimental approach has been developed for estimating both stress intensity factor (SIF) distributions and crack shapes during sub-critical flaw growth which includes all three modes of local deformation. After briefly tracing the development and features of the method and citing its limitations, recent results of the use of the method will be presented to support some fundamental observations on three dimensional sub-critical flaw growth.

KEY WORDS: Stress Intensity Factors, sub-critical crack growth, three dimensional cracked bodies, Experimental Methods.

## INTRODUCTION

In recent years two extensive bodies of literature have developed within the discipline of fracture mechanics. The first involves an accumulation of numerical analyses of three dimensional (3D) cracked body problems. These solutions deal primarily with elastic analyses of prescribed crack shapes and focus almost exclusively upon plane cracks. The second body of literature deals with sub-critical fatigue crack growth and focuses heavily upon experimental observations of an essentially one dimensional nature.

Most fractures in service are preceded by sub-critical crack growth which usually begins near a stress raiser of complex geometry. Consequently, the sub-critical flaw growth is almost never one dimensional (or even self-similar) but involves variable growth rates along flaw borders, curved crack fronts and, often, non-planar crack surfaces.

A major barrier to correlating experimentally observed sub-critical crack growth behavior with three dimensional numerical models has been the lack of knowledge of the flaw shapes and growth patterns in such problems. The common assumptions of simple flaw shapes with self-similar flaw growth are almost never experimentally observed over any appreciable crack growth increment. Moreover, substantial disagreement has existed between advocates of the continuum theory approach and materials scientists utilizing microscopic observations as to the role of local shear mode loads in the sub-critical crack growth process.

A survey of the current literature suggests that the role of local shear mode loads on sub-critical crack growth can be conveniently divided according to level of observation. There is much evidence that cracks parallel to slip planes in structural metals extend in small increments through enlargement under shear mode loads (Broek, 1974). In other situations, cleavage cracking appears to follow planes of maximum principal tensile stress. On the other hand, when macroscopic, or continuum level observations are made, fatigue crack growth appears to follow the plane of the maximum principal tensile stress in isotropic materials in the absence of cyclic shear mode loading (Cotterell, 1966; Cotterell and Rice, 1980; Smith, Peters and Kirby, 1981). When cyclic shear mode loading is employed macroscopically along with static mode I loading, there are cases where the crack plane may follow the shear mode plane (Otsuka and coworkers, 1981). However, this latter case seems to be the exception rather than the rule and the usual situation is that the main influence of the shear mode loading is to reorient the crack plane so that growth proceeds along the plane of the maximum principal tensile stress.

The present paper describes the progress in a continuing research program which is aimed towards modelling experimentally 3D sub-critical flaw growth at the continuum level so as to provide both flaw shapes and estimates of stress intensity distributions for such problems.

## THE METHOD

The modelling method under development involves two well known experimental tools:

i) Frozen stress photoelasticity - This method is used to obtain the flaw shape and an estimate of the SIF distribution.

ii) Moiré Interferometry - This method is used to evaluate SIF values at free surfaces and to provide displacement information.

### Frozen Stress Method

The analytical foundations for the photoelastic determination of stress intensity factor distributions due to mixed mode loading are described by Smith (1981) and elsewhere (Smith, Peters and Andonian, 1979). Consequently only the basic elements of the method will be repeated here.

For the case of Mode I loading, one begins with equations of the form:

$$\sigma_{ij} = \frac{K_I}{r^{1/2}} f_{ij}(\theta) + \sigma^0_{ij} \qquad i,j = n,z \tag{1}$$



for the stresses in a plane mutually orthogonal to the flaw surface and the flaw border referred to a set of local rectangular cartesian coordinates as pictured in Figure 1, where the terms containing $K_I$, the SIF, are identical to Irwin's Equations for the plane case and $\sigma^0_{ij}$ represent the contribution of the regular stresses to the stress field in the measurement zone. Since this zone does not include the crack surface, Eq. 1 need not satisfy the crack surface boundary conditions. This approach is often used in hybrid finite element work. The $\sigma^0_{ij}$ are normally taken to be constant for a given point along the flaw border, but may vary from point to point. Observing that stress fringes tend to spread approximately normal to the flaw surface (Figure 2), Eqs. 1 are evaluated along $\theta = \pi/2$ (Figure 1) and

$$\tau^{max}_{nz} = 1/2\,[(\sigma_{nn} - \sigma_{zz})^2 + 4\sigma^2_{nz}]^{1/2} \tag{2}$$

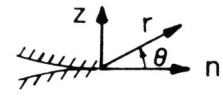


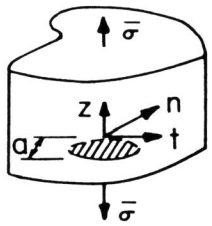


Fig. 1 General Problem Geometry and Notation

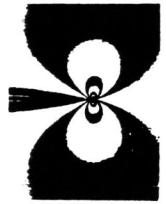

Fig. 2 Spreading of Fringes Away from Flaw Surfaces - Mode I

which, when truncated to the same order as Equations (1), leads to the two parameter equation:

$$\tau^{max}_{nz} = \frac{A}{r^{1/2}} + B \quad \text{where} \quad \begin{matrix} A = K_I/\sqrt{8\pi} \\ B = f(\sigma^0_{ij}) \end{matrix} \tag{3}$$

which can be rearranged into the normalized form

$$\frac{K_{AP}}{q(\pi a)^{1/2}} = \frac{K_I}{q(\pi a)^{1/2}} + \frac{f(\sigma^0_{ij})(8)^{1/2}}{q} \left(\frac{r}{a}\right)^{1/2} \tag{4}$$

where $K_{AP} = \tau_{max}(8\pi r)^{1/2}$ and, from the Stress-Optic Law, $\tau_{max} = Nf/2t'$ where N is the stress fringe order, f the material fringe value and t' the slice thickness in the t direction, q is the remote loading parameter (such as uniform stress, pressure, etc.) and a is the characteristic flaw depth. Equation (4) prescribes that, within the zone dominated by Equations (1) with $\sigma^0_{ij}$ as described above, a linear relation exists between the normalized apparent stress intensity factor and the square root of the normalized distance from the crack tip. Thus, one needs only to locate the linear zone in a set of photoelastic data and extrapolate across a very

near field non-linear zone (Jolles, McGowan and Smith, 1975) to the crack tip in order to obtain the SIF. A typical set of data are shown in Figure 3 for a slice removed from a nozzle corner crack in a reactor vessel model. LEFM data are filled circles (Region II). The region to the left of this data represents the near field non-linear zone (Region I). By following similar arguments, but not specifying $\theta = \pi/2$, equations for the Mixed Mode Case can also be developed (Smith, Peters and Andonian, 1979).

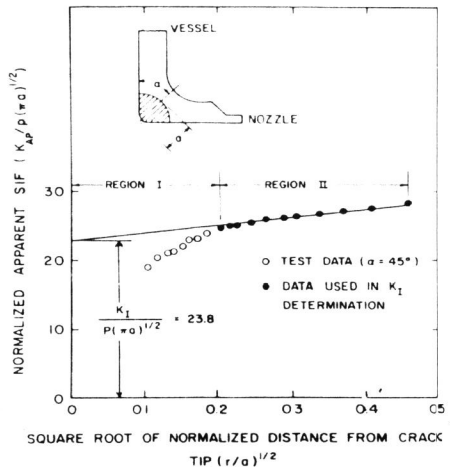


Fig. 3 Near Tip Photoelastic Data From a Frozen Slice

In order to obtain flaw shapes and an estimate of the SIF distribution for problems where neither are known a priori, we begin with fringe free cast sections of the part to be examined. We hold a sharp blade normal to the surface of the model part at the desired point and strike the blade with a hammer. A starter crack will propagate dynamically to a short distance from the blade tip and will then arrest itself. The parts of the model are then glued together, taking care that flaw borders are not to be located near glued surfaces, and the model is heated to critical temperature. Sufficient live load is applied above critical temperature to cause the crack to grow slowly. During growth, the crack is monitored through a glass oven port and when it reaches its approximate desired size, the load is reduced to terminate flaw growth, and the model is then cooled to room temperature. Upon unloading at room temperature, negligible recovery occurs and slices are removed with a band saw at intervals along the flaw border parallel to the nz plane (Fig. 1), coated with matching index fluid, and viewed through a crossed circular polariscope. The Tardy method is used to obtain fractional fringe orders. Optical data are then fed into a simple least square computer program for obtaining the straight line of best fit (Fig. 3) for use in estimating the normalized $K_1$ value.

Figure 4 shows near tip stress fringe loops for several different cases. Since the effect of Mode II is to rotate the Mode I fringe loops (compare (i) vs (ii)), the presence of Mode II is readily detectible in the stress fringe pattern. (Detection of Mode III requires viewing a subslice along the n axis.)

## Moiré Interferometry

Once the photoelastic data have been collected a linear diffraction grating is replicated on the surface of the slices according to a technique developed by Post (Post and Baracat, 1981). Assuming approximate reversibility of the displacement field in a stress-freezing material in the linear zone, the slices are annealed. The deformed active grating is interrogated by superposition of a reference grating of 1200 lines per millimeter. The resulting moire fringes describe the "negative" of the in-plane displacement field locked in the model during the stress freezing cycle.



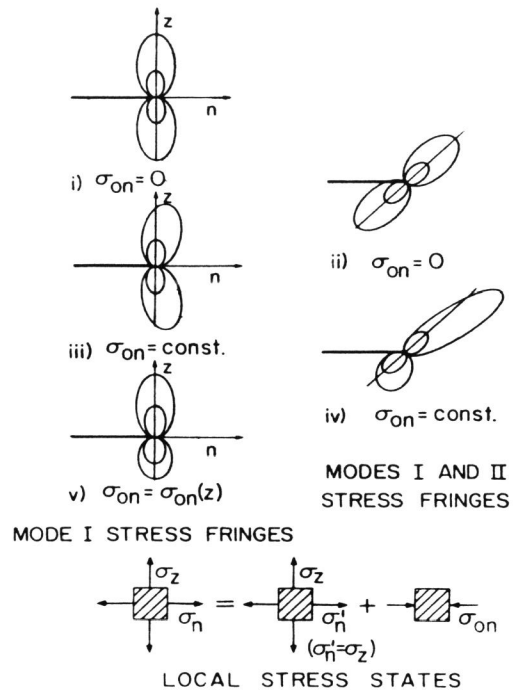


Fig. 4 Near Tip Stress Fringe Loops

The optical set-up for interrogating the annealed grating is shown in Fig. 5a (Smith, Post and Nicoletto, 1982). In practice, the reference grating is really a virtual grating.

The virtual grating, which is a three-dimensional array of walls of constructive and destructive interference, is generated wherever two collimated beams of light intersect and its frequency is a function of the angle of intersection as well as of the wavelength of the light.

The orientation of the optical elements used to create the virtual grating is pictured in Fig. 5b and the virtual grating itself is denoted as a hatched zone. The moire relationship gives

$$u_i = g_i N \qquad (i = n,z) \qquad (5)$$

where $g_i$ is the pitch of the grating having lines perpendicular to the $i$ direction and N is the moire fringe order.

According to LEFM the in-plane displacement field eqs. are (for plane strain)

$$u_z = \frac{2(1+\nu)}{E} K_{AP} \left\{\frac{r}{2\pi}\right\}^{1/2} \sin\frac{\theta}{2}\left[2 - 2\nu - \cos^2\frac{\theta}{2}\right] \qquad (6)$$

$$u_n = \frac{2(1+\nu)}{E} K_{AP} \left\{\frac{r}{2\pi}\right\}^{1/2} \cos\frac{\theta}{2}\left[1 - 2\nu + \sin^2\frac{\theta}{2}\right]$$

When only a linear grating normal to the z-axis is present and the measurements are taken along a line defined by $\theta = \frac{\pi}{2}$ in Fig. 2

$$K_{AP} = \frac{CN}{r^{1/2}} \qquad (7)$$

A plot of the normalized $K_{AP}$ vs. $(r/a)^{1/2}$ allows one to determine a region in which the data fall along a straight line. Its intersection with the

$K_{ap}$ axis yields an estimate of $K_I$ by moiré interferometry. A typical set of moiré data is shown in Fig. 5. The same approach using an orthogonal grating and measuring $u_n$ can also be used and may be more accurate, depending upon fringe geometry.

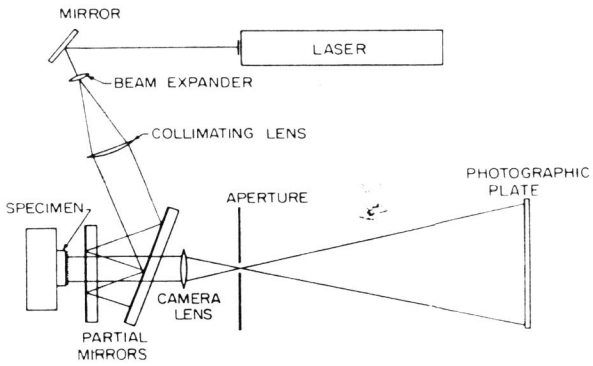


Fig. 5a Optical Arrangement for Moiré Interferometric Measurements

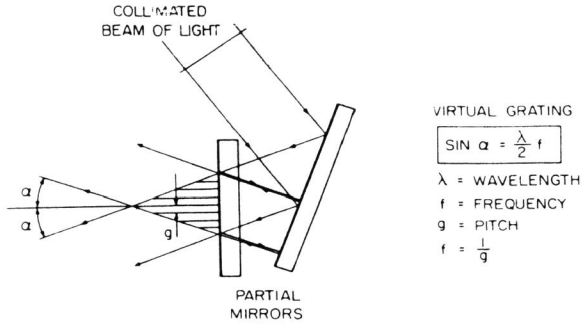


Fig. 5b Virtual Grating Formed by an Adjustable Wedge System

## APPLICATION OF THE METHOD

In order to illustrate some features of the method, we consider its application to a problem which was briefly mentioned by Smith (1981). The problem consists of a crack initially planar, at the reentrant corner of the intersection of a thick walled tube with a thin walled cylinder where both are subjected to internal pressure (Fig. 7). When slices mutually orthogonal to the flaw border and the flaw surface were taken at the intersection of the flaw border with the inner wall of the tube (point n in Fig. 7) stress fringe loops of the form of Fig. 4(iii) were obtained, indicating pure Mode I loading. However near point m, fringe loops of the form of Fig. 4(iv) were obtained prior to flaw growth, suggesting the presence of both Modes I and II near point m. When the pressure was increased on a second cracked model sufficient to grow the crack, it grew in its plane in the neighborhood of n but turned to a new orientation as it grew near m. After turning near m, fringes of the form shown in Fig. 4(v) were observed. This suggests that stably growing cracks reorient themselves to eliminate shear modes in isotropic bodies.

When linear gratings were applied to stress frozen slices taken from the interior and at the outer surface, it was found that upon annealing, the SIFs obtained from the moiré data using plane strain displacement equations agreed with the photoelastic data to within experimental scatter for the interior slices but were generally slightly higher. On the outer surface, the extrapolated value of the photoelastic SIF fell in between the two moire SIF values computed from plane strain and plane stress displacements respectively. The fact that plane stress values are not achieved at the surface photoelastically is probably due to the bulk constraint of the internal material. Further details of this study may be found (Smith, Post and Nicoletto, 1982; and Smith, Post and Haitt, 1981).



## LIMITATIONS OF METHOD

The method described above is not without limitations. We note them briefly as follows:

1) Gross elastic behavior of an incompressible material must produce negligible error in flaw shape and only slight elevation of the SIF.

2) Starter crack geometries for model and prototype must be the same.

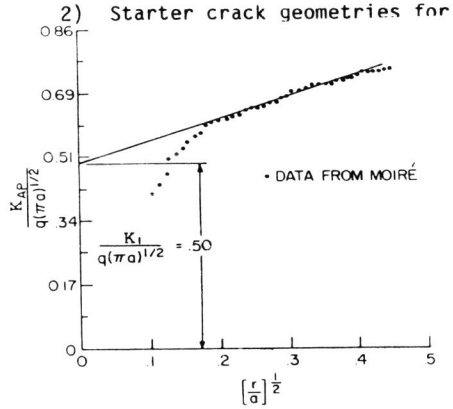


Fig. 6 Near Tip Moiré Date From In-Plane Displacements

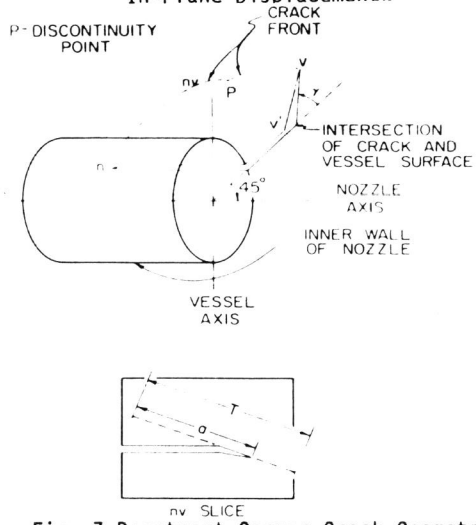


Fig. 7 Reentrant Corner Crack Geometry

3) The accuracy of shear mode SIF determinations is only approximately half that of Mode I SIF determinations.

4) No fatigue overloads are permitted in the prototype loading.

5) Flaw border length must be sufficiently large that any crack closure in the prototype is confined to the surface layers of the body (i.e. fatigue enhancement effects are negligible).

6) Some limitation on the load spectrum if part of the spectrum is in compression.

The first four of the above items relate either to constraints of the method itself or accrue from repeated observations resulting from the application of the method to 3D cracked body problems. Item 5 is an obvious consequence of comparing cracks grown by fatigue loading in prototypes with cracks grown under monotonic loads in the photoelastic models. There is evidence, however, that such conditions do often exist (Smith and Peters, 1978a; Smith and Peters, 1978b; Evans and Fuller, 1974). Item 6 is included for the sake of completeness. Actually, to date, insufficient information is available to accurately assess the load spectrum effects.

Despite the above noted limitations, the method appears to offer a potential for opening the way to the

numerical analyst for providing improved predictions of 3D sub-critical flaw geometries and associated SIF distributions.

## ACKNOWLEDGEMENTS

The authors wish to acknowledge the influence of the work of colleagues as referenced, the advice of D. Post and the support of the staff and facilities of the Department of Engineering Science and Mechanics at Virginia Polytechnic Institute and State University and the support of the National Science Foundation through Grant No. MEA 811-3565.

## REFERENCES

Broek, D., (1974). Elementary engineering fracture mechanics, Noordhoff International.

Cotterell, B., (1966). International Journal of Fracture, Vol. 2, No. 3, pp. 526-533.

Cotterell, B. and Rice, J. R., (1980). International Journal of Fracture, Vol. 16, No. 2, pp. 155-170.

Evans, A. G. and Fuller, E. R., (1974). Crack propagation in ceramic materials under cyclic loading conditions", Metallurgical Transactions, Vol. 5, pp. 27-33.

Jolles, M., McGowan, J. J. and Smith, C. W., (1975). Use of a hybrid computer assisted photoelastic technique for stress intensity factor determination in three dimensional problems, Computational Fracture Mechanics, ASME Sp. Publ. E. F. Rybicki and S. E. Benzley, Eds., pp. 83-102.

Otsuka, A., Mori, K., Ohshima, T. and Tsuyama, S., (1981). Mode II fatigue crack growth in aluminum alloys and mild steel", Advances in Fracture Research, Vol. 4, D. Francois et al, Eds., pp. 1851-1858.

Post, D. and Baracat, W. A., (1981). Journal of Experimental Mechanics, Vol. 21, No. 3, pp. 100-104.

Smith, C. W. and Peters, W. H., (1978). Experimental observations of three dimensional geometric effects in cracked bodies, Developments in Theoretical and Applied Mechanics, Vol. 9, pp. 225-234.

Smith, C. W. and Peters, W. H., (1978). Prediction of flaw shapes and stress intensity distributions in 3D problems by the frozen stress method, Preprints of Fifth International Conference on Experimental Stress Analysis, pp. 861-864.

Smith, C. W. Peters, W. H. and Andonian, A. T., (1979). Journal of Engineering Fracture Mechanics, Vol. 13, pp. 615-629.

Smith, C. W., Peters, W. H. and Kirby, G. C., (1981). Observations on crack shapes and stress intensity distributions during stable flaw growth, Analytical and Experimental Fracture Mechanics, G. C. Sih and M. Mirabile, Eds., Sijthoff-Noordhoff, pp. 699-710.

Smith, C. W., (1981). Determination of mixed mode stress intensity factors by photoelasticity in three dimensional problems, Mixed Mode Crack Propagation, G. C. Sih and P. S. Theocaris, Eds., Sijthoff-Noordhoff, p. 285-296.

Smith, C. W., Post, D. and Haitt, G., (1981). Displacement measurements around cracks in three dimensional problems by a hybrid experimental technique, Proceedings of SESA Annual Meeting, pp. 314-320.

Smith, C. W., Post, D. and Nicoletto, G., (1982). Prediction of sub-critical crack growth data from model experiments, Proceedings of the Eleventh Southeastern Conference on Theoretical and Applied Mechanics, pp. 167-180.